THE JOURNAL OF PHYSICAL CHEMISTRY B LETTERS

2006, *110,* 17702−17705
Published on Web 08/22/2006

Grazing Angle Mirror-Backed Reflection (GMBR) for Infrared Analysis of Monolayers on Silicon

Hong-Bo Liu,[†] Shou-Jun Xiao,*[,†] Ya-Qing Chen,[†] Jie Chao,[†] Jing Wang,[†] Yue Wang,[†] Yi Pan,[†] Xiao-Zeng You,[†] and Zhong-Ze Gu[‡]

State Key Laboratory of Coordination Chemistry, School of Chemistry and Chemical Engineering, Nanjing University, Nanjing 210093, China, and State Key Laboratory of Molecular and Biomolecular Electronics, Southeast University, Nanjing 210096, China

Received: June 5, 2006; In Final Form: August 8, 2006

An easy handling infrared measurement, grazing angle mirror-backed reflection (GMBR), has been established to analyze the silicon-based organic monolayer. Theoretical prediction gave the optimal configuration with p-polarized irradiation near a grazing angle 78.1° of incidence. Experimental measurement of hydrogen-terminated, undecylenic acid (UA) and *N*-hydroxysuccinimide (NHS) functionalized silicon (111) surfaces showed good signal peaks and reproducibility.

Fabrication of organic monolayer on silicon wafer attracts much attention in molecular, nano, and microelectronics.[1−5] With the development of monolayers based on Si−C and Si−O−C bonds, more potential applications are emerging, such as biochips, (bio)chemical sensors, molecular recognition, solar cells, chemical and electrical surface passivation, and control of photopatterning.[6−10] Infrared spectroscopy (IRS) is a powerful, nondestructive tool for studying the grafted molecular structure and for qualifying the monolayer performance, which are crucial in further fabrication of nanodevices.[11,12] Due to the low sensitivity of standard transmission IRS for organic monolayer on silicon, one usually has to rely on the multiple internal reflection (MIR),[13] in which the monolayer was fabricated on an attenuated total reflection (ATR) silicon crystal with 45° bevel angles at each end and the sensitivity was increased by multiple reflections. This technique gives a good analysis result, but the costly ATR crystal cannot be used technically and economically as silicon wafer for further device fabrication. A recently developed setup for analysis of monolayer on silicon was Otto's ATR configuration[14] (a commercial Harrick accessory GATR is available now) by directing the IR beam through the higher-refractive-index ATR crystal, germanium, to the monolayer/Si interface at an incident angle larger than the critical angle 60° to ensure a total reflection.[15,16] The sensitivity enhancement was previously obtained when a thin film is sandwiched between two high-refractive-index materials.[17] In this configuration, the monolayer-grafted silicon surface was pressed against the Ge crystal to have an intimate contact, and the pressure should be carefully controlled to maximize the surface sensitivity. A notable advantage of this measurement is that there is no strict requirement for the geometry of silicon wafer. The p-polarized transmission at the Brewster angle (73.6° for silicon) for characterization of an organic monolayer has also been investigated.[18] For example, Chabal et al. discussed the infrared spectra of hydrogen- and chlorine-terminated silicon surface in detail.[19] External reflection was rarely used to analyze the silicon-based organic monolayer.[20,21] Zuilhof and co-wokers showed weak signal of the C−H stretching but did not show any signal of the Si−H stretching.[21] In fact, due to the split of infrared rays on the air/Si interface, the energy of the transmitted beam at the external reflection setup is lost, and therefore, the external reflection is not sensitive enough to characterize organic monolayers. Compensation of the energy loss can be performed by reflecting back the transmitted infrared rays with a metal film deposited on the other side of silicon wafer. An example was given for analysis of the oxide layer in the metal oxide semiconductor (MOS) structure widely used in microelectronics.[22] However, metal deposition is a destructive process for characterization of the monolayer functionalized sample. It would change the monolayer structure due to the penetration and chemical reaction of metal atoms with surface molecules.[6,23] Mirror-backed reflection measurement had been of interest for thickness determination of photoresist films, as it avoids interference oscillation relative to normal-incidence transmission.[24,25] Here, we introduce GMBR for IR analysis of silicon-based monolayers by placing a mirror behind the double-side-polished silicon wafer in the grazing-angle external reflection experiments. Energy compensation simultaneously increases the band intensity and the signal-to-noise ratio (SNR) for both p- and s-polarization spectra. In this report, numerical and experimental analyses were done to prove its feasibility. The GMBR setup provides the advantage of easy handling and flexible sampling with no restriction of silicon geometry as the commercial GATR does. However, GMBR is superior in nondestruction of the grafted monolayer.

Figure 1a shows the layout of the GMBR measurement accomplished in grazing-angle external reflection accessory with a fixed 80° incidence. The incident infrared light is split into two parts as reflection and transmission when it reaches the silicon surface. Subsequently, the transmission light passing through silicon is reflected back by the gold mirror, and then it

* Corresponding author. E-mail: sjxiao@nju.edu.cn. Tel: +86-25-83595706. Fax: +86-25-83314502.
[†] Nanjing University.
[‡] Southeast University.

10.1021/jp063467q CCC: $33.50

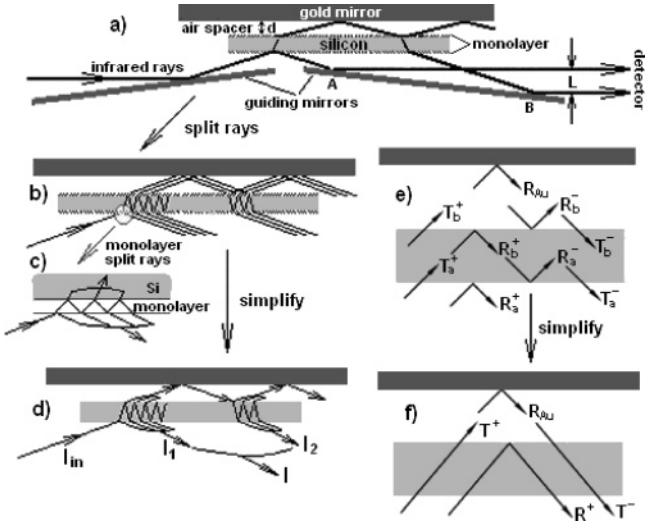

Figure 1. (a) Experimental setup for GMBR. (b) Multiple reflection and multiple transmission taken place both in silicon and in monolayer. (c) Amplification of multiple reflection and multiple transmission in monolayer. (d) Simplified three-media model for calculation with air/Si(monolayer)/air; I_{in} and I denote the incident and emergent light intensity; I_1 and I_2 are the reflection and double-transmission light respectively. (e) Symbols of reflectance (R) and transmittance (T) at the interface for lower (subscript a) and upper (subscript b) surfaces of silicon wafer; the superscript + indicates the light traveling direction from air/Si_a interface to Si_b/air interface, and − for the opposite direction (from air/Si_b to Si_a/air interface). Si_a and Si_b denote the lower and upper silicon surfaces, respectively. R_{Au} denotes the reflectance of gold mirror. (f) Sum reflectance (R^+) and transmittance (T^+, T^-) for whole silicon wafer.

traverses silicon again. Following the increment of the air spacer between gold mirror and silicon to 1 mm, the distance between the first reflection spot (point A) and the double-transmission spot (point B) on the guiding mirror is about 23 mm, and the span width (L) of the IR beam to enter the detector is about 2 mm. Since the guiding mirrors in the grazing-angle accessory are 70 mm long, most reflection and double-transmission light can reach the detector by adjusting the accessory with a suitable height (see Figure S1 in Supporting Information). As a result, a relatively higher sensitivity can be obtained.

Numerical simulation was carried out to analyze the sensitivity of GMBR and Brewster angle transmission measurements, and the simulated optimum parameters were examined in our experiments. As shown in Figure 1b,c, all multiple reflections and multiple transmissions in both monolayer and silicon wafer are taken into account. The calculation was simplified with a three-media model air/Si/air in Figure 1d, where in this model the monolayer-modified silicon (monolayer/Si in Figure 1c) is integrated as a single interface, but its Fresnel coefficient calculated with eq 4 is different from the bare air/Si interface. In addition, no interference was considered for silicon wafer.[24,26] Fresnel amplitude coefficient of interface is the ratio of electric-field amplitude in medium j to that in medium i derived from the description of Hansen[27]

$$r_{ij}^{s} = \frac{\xi_i - \xi_j}{\xi_i + \xi_j} \quad r_{ij}^{p} = \frac{\hat{n}_j^2 \xi_i - \hat{n}_i^2 \xi_j}{\hat{n}_j^2 \xi_i + \hat{n}_i^2 \xi_j} \tag{1}$$

$$t_{ij}^{s} = \frac{2\xi_i}{\xi_i + \xi_j} \quad t_{ij}^{p} = \frac{2\hat{n}_i \hat{n}_j \xi_i}{\hat{n}_j^2 \xi_i + \hat{n}_i^2 \xi_j} \tag{2}$$

$$\xi_i = \hat{n}_i \cos \varphi_i = \sqrt{\hat{n}_i^2 - \hat{n}_0^2 \sin^2 \varphi_0} \tag{3}$$

where $\hat{n} = n + ik$ is the complex refractive index. The subscript 0 denotes incident medium and superscripts s and p for s- and p-polarized irradiation. If an isotropic layer with finite thickness is located at the planar interface of two semi-infinite media, the Fresnel coefficients can be rewritten in the form

$$r_{123}^{p,s} = \frac{r_{12}^{p,s} + r_{23}^{p,s} e^{2i\beta}}{1 + r_{12}^{p,s} r_{23}^{p,s} e^{2i\beta}} \quad t_{123}^{p,s} = \frac{t_{12}^{p,s} t_{23}^{p,s} e^{i\beta}}{1 + r_{12}^{p,s} r_{23}^{p,s} e^{2i\beta}} \tag{4}$$

$$\beta = 2\pi k d \xi_2 \tag{5}$$

where $r_{ij}^{p,s}$ and $t_{ij}^{p,s}$ are the two-phase Fresnel coefficients calculated by eqs 1 and 2, respectively; β is the phase shift of the electromagnetic wave after one pass through the film; k is the wavenumber of incident light; d is the thickness of film. The transmittance and reflectance related to Fresnel coefficients are described as

$$R_{1(2)3}^{p,s} = |r_{1(2)3}^{p,s}|^2 \qquad T_{1(2)3}^{s} = \frac{\mathrm{Re}\xi_3}{\xi_1} |t_{1(2)3}^{s}|^2$$

$$T_{1(2)3}^{p} = \frac{\mathrm{Re}(\xi_3/\hat{n}_3^2)}{\xi_1} |\hat{n}_3 t_{1(2)3}^{p}|^2 \tag{6}$$

The reflectance ($R^{+(-)}{}_{a(b)}$) and transmittance ($T^{+(-)}{}_{a(b)}$) at the interface of air/Si and air/monolayer/Si shown in Figure 1e can be obtained from eq 6. The subscripts a and b denote the lower and upper faces of silicon, and the superscripts + and − indicate the light traveling directions. The sum reflectance (R^+) and transmittance (T^+, T^-) of silicon wafer (Figure 1f) can be described by the following equations:[30, 32]

$$R^+ = R_a^+ + \frac{T_a^+ R_b^+ T_a^-}{1 - R_a^- R_b^+} \qquad T^+ = T^- = \frac{T_a^+ T_b^+}{1 - R_a^- R_b^+} \tag{7}$$

The total output light intensity can be written as

$$I = R' I_{in} = I_1 + I_2 = R^+ I_{in} + (T^+ R_{Au} T^-) I_{in} \tag{8}$$

$$R' = R^+ + T^+ R_{Au} T^- \tag{9}$$

Here, I_{in}, I_1, and I_2 are the light intensities of the incident, reflection, and double-transmission light, respectively (Figure 1d). R' is the reflectance of output light, which equals the ratio of emergent light intensity to incident light intensity. R_{Au} is the reflectance of gold mirror. The absorbance (A) and absorption depth ($\Delta R'$) is defined through

$$A = -\log_{10}(I/I_0) = -\log_{10}(R'/R_0') \tag{10}$$

$$\Delta R' = R_0' - R' \tag{11}$$

where I and R' with and without subscript 0 correspond to the output light intensity and reflectance calculated without and with the monolayer.

For numerical analysis, the following parameters were selected as typical: $n_1 = 1.0$ (air), $n_3 = 3.42$ (silicon substrate), $n_{Au} = 3.2 + 20i$ (gold mirror), and $n_\infty = 1.46$.[35] Since our goal is to characterize the molecular monolayer on silicon using GMBR measurement, we choose the UA monolayer as an example for numerical analysis. The thickness of the UA monolayer is $d = 0.7$ nm.[35] The complex refractive index of the monolayer can be determined from the experimental spectra using the iterative fitting method of Buffeteau[33] (see Supporting

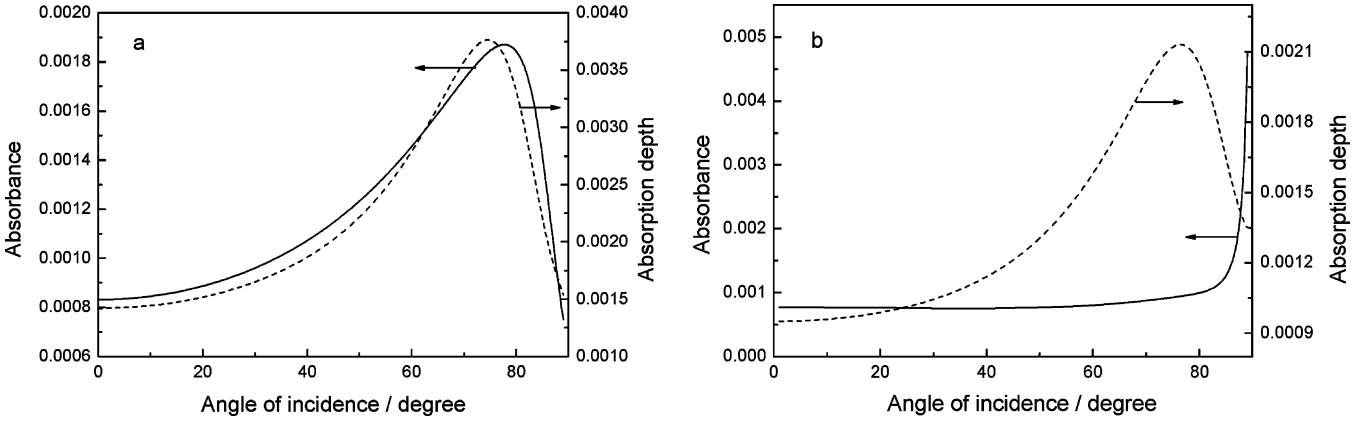

Figure 2. Calculated absorbance (A, solid line) and absorption depth ($\Delta R'$, dashed line) versus angle of incidence for p-polarized irradiation with (a) mirror-backed reflection and (b) transmission measurement for the UA monolayer at $\nu_{as}(CH_2) = 2927$ cm^{-1}.

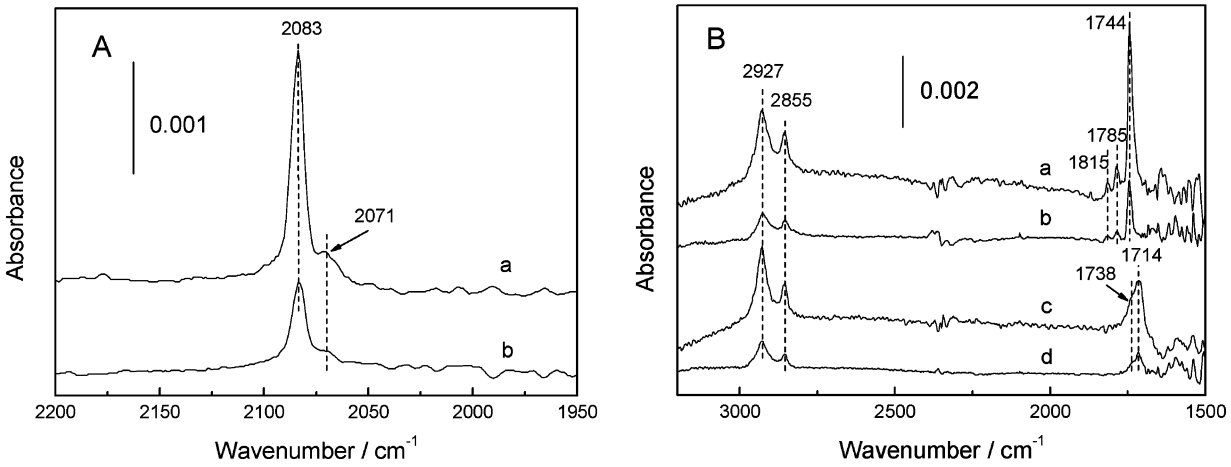

Figure 3. Experimental p-polarized spectra: (A) monohydrogen-terminated Si(111) surface by (a) GMBR and (b) Brewster angle transmission at 74°; (B) surfaces modified with (a,b) NHS and (c,d) UA monolayers by (a,c) GMBR and (b,d) Brewster angle transmission. The regions 2400−2280 cm^{-1} and 1500−1800 cm^{-1} are affected by CO_2 and H_2O, respectively. Spectra are shown after subtraction of water and CO_2.

Information, Section 2). The UA monolayer is composed of ten methylenes and one carboxyl group; thus, we select the overwhelming methylene species as the monolayer for numerical analysis. The normalized experimental p- and s-polarized spectra of the $\nu_{as}(CH_2)$ mode (2927 cm^{-1}) were used for iterative simulation. The monolayer was treated as a uniaxially oriented layer, and the optical properties can be described by in-plane ($\hat{n}_{2x} = \hat{n}_{2y}$) and out-of-plane ($\hat{n}_{2z}$) complex refractive indexes. From Buffeteau's iterative simulation at a fixed 80° of incidence, the complex refractive indexes were determined as follows: $\hat{n}_{2x} = \hat{n}_{2y} = 1.52 + 0.39i$ and $\hat{n}_{2z} = 1.44 + 0.23i$. In this case, the refractive angle inside monolayer (φ_2) was determined with $\hat{n}_{2z}$ ($n_1 \sin \varphi_1 = \hat{n}_{2z} \sin \hat{\varphi}_2$) especially for p-polarization. In other equations, $\hat{n}_2$ was replaced by $\hat{n}_{2x}(\hat{n}_{2y})$.[33,34]

The above iterated complex refractive indexes were then used to calculate the optimum configuration of the GMBR setup. The result of numerical analysis from incident angle 0° to 89° for p-polarization is shown in Figure 2a, where the absorbance and absorption depth of the monolayer is drawn against the incident angle. The band intensity is determined by the absorbance, and SNR is proportional to the absorption depth in a detector noise-limited spectrometer.[18] The angular dependence of absorbance for p-polarization exhibits the highest value at 78.1°, close to the maximum absorption depth, 74.9°. For s-polarization, both absorbance and absorption depth decrease smoothly with increasing angle of incidence, but the band intensity is far less than that of p-polarization (Figure S4-a in Supporting Information). The coincidence of maximum absorbance and absorption depth for both p- and s-polarization is due to the energy compensation by placing a mirror behind the silicon wafer, which facilitates the choice of the optimum angle of incidence. These results show that the optimum measurement can be achieved in the mirror-backed system by using the p-polarized irradiation at grazing angles of incidence. For the transmission setup at Brewster angle, we used the same numerical analysis method but only considered the transmission signals (Figure 2b). The absorbance increases very slowly in the incident angles from 0° to Brewster angle 73.6° and increases sharply after a grazing angle 80°, but the absorption depth reaches its maximum at Brewster angle of 73.6° and then decreases steeply (Figure 2b). The simulated absorbance at 80° in GMBR (Figure 2a) is 0.018, twice that in the Brewster angle transmission (0.009 from Figure 2b), in accordance with our experimental results. The external reflection measurement is hardly used to detect the silicon-based monolayer for its low absorption depth at grazing angles (the simulated results are shown in Figure S5 in Supporting Information). It should be noted that the spectra calculated with a double-side-polished wafer is different from the single-side-polished one.[26]

Experimental spectra of GMBR and Brewster angle transmission are given in Figure 3A,B for comparison (for experimental details, please see Supporting Information). Three typical structures of Si−H (curves a and b in Figure 3A), UA (c and d in Figure 3B), and NHS (a and b in Figure 3B) monolayer species on silicon wafer are exemplified. Hydrogen-terminated silicon surface is the basis for fabrication of Si−C bonded

monolayer, and its strong IR stretching mode (~2100 cm^{-1}) provides a suitable sample for testing the sensitivity of IR measurement. The carboxylic acid terminated monolayer (UA), and its subsequently derivative NHS monolayer, frequently used for immobilization of biomolecules and fabrication of biochips,[7,28] are chosen for testing organic monolayers with featured absorption at ~1700 cm^{-1}. The vibration bands in this region can exclusively distinguish the ambiguity of the C−H stretching at 2800−2980 cm^{-1}, where the contaminated hydrocarbons also contribute to the absorption. The NHS species possesses three specifically coordinated peaks, 1815, 1785, and 1744 cm^{-1}.[7,28] It is an excellent marker for testing our IR setup. The Si−H band intensity in Figure 3A at 2083 cm^{-1} by GMBR (Figure 3Aa) is about 2 times higher than that by the Brewster angle transmission (Figure 3Ab), due to the contribution of both reflection and double-transmission light to absorbance. It is consistent with the result of our numerical analysis. The Si−H stretching mode 2083 cm^{-1}, normal to the surface, is characteristic of an ideal monohydrogen-terminated Si(111) surface.[29] A small shoulder peak at 2071 cm^{-1} is also observed in the p-polarized spectra, most probably assigned to the parallel portion of the Si−H stretching to the surface.[30,31] The intensity difference of the two peaks can be explained with the existence of both surface normal (absolutely overwhelming portion) and parallel (trace portion) components in p-polarized rays when traveling through the surface at 80° incidence.[32] By the way, easy contamination of hydrocarbons from the air to silicon surface after NH_4F treatment[36] exhibits asymmetric (ν_{as} = 2921 cm^{-1}) and symmetric (ν_s = 2852 cm^{-1}) stretching modes of CH_2 and an asymmetric (ν_{as} = 2960 cm^{-1}) stretching shoulder of CH_3 (data not shown). In Figure 3B, all four spectra show C−H stretching at relatively higher wavenumbers of 2927 and 2855 cm^{-1}, due to the disordered and noncrystalline monolayers on silicon.[37,38] It was reported that the crystalline self-assembly monolayers (SAMs) of 1-decanethiol on Au had CH_2 stretching bands at 2920 and 2850 cm^{-1} but disordered SAMs of undecylenic acid thiol on Au at 2925 and 2853 cm^{-1} due to the presence of carboxyl group.[39] Figure 3Bc,d exhibits the main carboxylic acid stretching at 1714 cm^{-1}; however, a shoulder peak at 1738 cm^{-1} is also observable, which can be assigned to the byproduct of a reaction between carboxylic acid (−COOH) and Si−H (see Supporting Imformation, Scheme S1).[40] The side reaction may also contribute to the disorder of the monolayers. Obviously, after NHS functionalization, the three specifically coordinated peaks (1815, 1785, and 1744 cm^{-1}), assigned to the succinimidyl ester, appear in Figure 3Ba,b. The spectra measured by GMBR in Figure 3Ba and c, similar to the Si−H measurement, have stronger signals than by transmission near the Brewster angle in Figure 3Bb and d. To get a good spectrum, the size of the air spacer is critical, because a small spacer will generate interference fringes, but a larger one will lose the double-transmission light and thus lose the intensity. The spacer size used for Figure 3 is 1 mm, and the detector is DTGS. It is also revealed that the interference fringes are stronger when liquid nitrogen cooled MCT detector is used (see Supporting Information, Figure S6).

In summary, we have employed the GMBR measurement to infrared analysis of silicon-based monolayers. This way combines the external reflection and transmission together for IR beam transparent substrates. It is believed that by changing the incident angle we can study the molecular orientation with the analysis of p- and s-polarized spectroscopy. The GMBR-based IR spectroscopy has been proven to be an effective and easy way to handle characterization of organic monolayers on silicon.

Acknowledgment. The authors thank the critical reading and helpful suggestions of the reviewer. Mr. Hong-Qi Shi's help in the FITR measurements is appreciated. This work was supported by NSFC no. 20571042.

Supporting Information Available: Experimental details; determination of the refractive index of UA monolayer; experimental and simulated spectra; numerical analysis of s-polarization for GMBR and transmission measurement; numerical analysis for external reflection measurement; experimental interference fringes affected by the air spacer and the detector. This material is available free of charge via the Internet at http://pubs.acs.org.

References and Notes

(1) Rakshit, T.; Liang, G.-C.; Ghosh, A. W.; Datta, S. *Nano Lett.* **2004**, *4*, 1803.
(2) Lenfant, S.; Krzeminski, C.; Delerue, C.; Allan, G.; Vuillaume, D. *Nano Lett.* **2003**, *3*, 741.
(3) Carroll, R. L.; Gorman, C. B. *Angew. Chem., Int. Ed.* **2002**, *41*, 4378.
(4) Faber, E. J.; de Smet, L. C. P. M.; Olthuis, W.; Zuilhof, H.; Sudholter, E. J. R.; Bergveld, P.; Berg, A. v. d. *ChemPhysChem* **2005**, *6*, 2153.
(5) Richter, C. A.; Hacker, C. A.; Richter, L. J. *J. Phys. Chem. B* **2005**, 109, 21836.
(6) Buriak, J. M. *Chem. Rev.* **2002**, *102*, 1271.
(7) Voicu, R.; Boukherroub, R.; Bartzoka, V.; Ward, T.; Wojtyk, J. T. C.; Wayner, D. D. M. *Langmuir* **2004**, *20*, 11713.
(8) Lasseter, T. L.; Clare, B. H.; Abbott, N. L.; Hamers, R. J. *J. Am. Chem. Soc.* **2004**, *126*, 10220.
(9) Bent, S. F. *Surf. Sci.* **2002**, *500*, 879.
(10) Onclin, S.; Ravoo, B. J.; Reinhoudt, D. N. *Angew. Chem., Int. Ed.* **2005**, *44*, 6282.
(11) Hirschmugl, C. J. *Surf. Sci.* **2002**, *500*, 577.
(12) Chabal, Y. J.; Raghavachari, K. *Surf. Sci.* **2002**, *502*−*503*, 41.
(13) Harrick, N. J. *Internal Reflection Spectroscopy*; Harrick Scientific Corporation: New York, 1979.
(14) Otto, A. *Z. Phys.* **1968**, *216*, 398.
(15) Lummerstorfer, T.; Hoffmann, H. *Langmuir* **2004**, *20*, 6542.
(16) Milosevic, M.; Berets, S. L.; Fadeev, A. Y. *Appl. Spectrosc.* **2003**, *57*, 724.
(17) Brendel, R. *J. Appl. Phys.* **1992**, *72*, 794.
(18) Tolstoy, V. P.; Chernyshova, I. V.; Skryshevsky, V. A. *Handbook of Infrared Spectroscopy of Ultrathin Films*; Wiley-Interscience: New York, 2003.
(19) Webb, L. J.; Rivillon, S.; Michalak, D. J.; Chabal, Y. J.; Lewis, N. S. *J. Phys. Chem. B* **2006**, *110*, 7349.
(20) Hoffmann, H.; Mayer, U.; Krischanitz, A. *Langmuir* **1996**, *11*, 1304.
(21) Sun, Q.-Y.; de Smet, L. C. P. M.; Lagen, B. V.; Giesbers, M.; Thune, P. C.; Engelenburg, J. V.; de Wolf, F. A.; Zuilhof, H.; Sudholter, E. *J. Am. Chem. Soc.* **2005**, *127*, 2514.
(22) Brendel, R.; Hezel, R. *J. Appl. Phys.* **1992**, *71*, 4377.
(23) Jun, Y.; Zhu, X.-Y. *J. Am. Chem. Soc.* **2004**, *126*, 13224.
(24) Brendel, R. *J. Appl. Phys.* **1991**, *69*, 7395.
(25) Chrostopher, J. G.; Glenn, R. H.; James, W. T. *Anal. Chem.* **1994**, *66*, 1015.
(26) Hasegawa, T.; Nishijo, J.; Kobayashi, Y.; Umemura, J. *Bull. Chem. Soc. Jpn.* **1997**, *70*, 525.
(27) Hansen, W. N. *J. Opt. Soc. Am.* **1968**, *58*, 380.
(28) Guo, D.-J.; Xiao, S.-J.; Xia, B.; Wei, S.; Pei, J.; Pan, Y.; You, X.-Z.; Gu, Z.-Z.; Lu, Z. *J. Phys. Chem. B* **2005**, *109*, 20620.
(29) Higashi, G. S.; Chabal, Y. J.; Trucks, G. W.; Raghavachari, K. *Appl. Phys. Lett.* **1990**, *56*, 656.
(30) Jakob, P.; Chabal, Y. J. *J. Chem. Phys.* **1991**, *95*, 2897.
(31) Kakuda, H.; Hasegawa, T. *Chem. Phys. Lett.* **2005**, *415*, 172.
(32) Hasegawa, T. *J. Phys. Chem. B* **2002**, *106*, 4112.
(33) Buffeteau, T.; Blaudez, D.; Pere, E.; Desbat, B. *J. Phys. Chem. B* **1999**, *103*, 5020.
(34) Yamamoto, K. Ph.D. Thesis, Case Western Reserve University, 1994, no. 9501975.
(35) Linford, M. R.; Fenter, P.; Eisenberger, P. M.; Chidsey, C. E. D. *J. Am. Chem. Soc.* **1995**, *117*, 3145.
(36) Ling, L.; Kuwabara, S.; Abe, T. *J. Appl. Phys.* **1993**, *73*, 3018.
(37) Porter, M. D.; Bright, T. B.; Allara, D. L.; Chidsey, C. E. D. *J. Am. Chem. Soc.* **1987**, *109*, 3559.
(38) Perring, M.; Dutta, S.; Arafat, S.; Mitchell, M.; Kenis, P.; Bowden, N. B. *Langmuir* **2005**, *21*, 10537.
(39) Chidsey, C.; Loiacono, D. N. *Langmuir* **1990**, *6*, 682.
(40) Asanuma, H.; Lopinski, G. P.; Yu, H.-Z. *Langmuir* **2005**, *21*, 5013.